Imaging Geo-synchronous Satellites with the AEOS Telescope

Douglas A. Hope[1], Stuart M. Jefferies[1,2] and Cindy Giebink[1]
[1]*Institute for Astronomy, University of Hawaii, Advanced Technology Research Center*
34 Ohia Ku Street
Pukalani, Maui HI 96768, USA
Ph: (808) 573 9540, Fax: (808) 573-9557
dhope@.ifa.hawaii.edu

[2]*Steward Observatory, University of Arizona, 933 N. Cherry Ave., Rm. N204*
Tucson, AZ 85721, USA
Ph: (520) 621-2288, Fax: (520) 621-1532

ABSTRACT

The USA has significant civilian and military assets in geostationary orbit. High-resolution, ground-based imaging of these assets enables us to monitor in detail their health and safety and to detect the presence of any foreign micro-satellites that might be in proximity. Although adaptive optics compensation of ground-based imagery imparts some level of mitigation of the deleterious effects due to the Earth's turbulent atmosphere, the correction is far from optimal and there is usually ample room for further improvement in resolution through image post processing. Here we show that significant gains in image fidelity and detection sensitivity can be achieved during the image post processing by the injection of prior information on the wave-front phases via wave-front sensing data and wave/phase-diverse data. The gains are such that it is possible that AEOS could become a practical resource for high-fidelity imaging and detection of GEO targets.

1. INTRODUCTION

The USA has significant civilian and military assets in geostationary orbit. Monitoring their health and safety is a pimary goal of space situational awareness (SAA). Important information for achieving SAA includes high-resolution imagery of the primary target, which facilitates detection of any potentially threatening micro-satellites (linear size $\leq$ 25 cm) that might be in proximity. Obtaining this information from the ground requires a large aperture telescope equipped with adaptive optics (AO) correction[1] to compensate for distortions in the incoming wave front caused by turbulence in the Earth's atmosphere. However, this compensation is never complete and image restoration methods (e.g., blind deconvolution techniques) are required to obtain target imagery of the highest possible resolution.

Turbulence in the atmosphere acts as a randomly fluctuating spatial filter that blurs the observed image. The atmospheric point-spread-function (PSF) characterizes this blur. The amount of diversity in the morphology of the PSF (variability as a function of time) depends on the strength of the turbulence as well as the exposure time. The diversity is the basis of multi-frame blind image deconvolution (MFBD) methods, which estimate a target scene common to all data frames along with each realization of the atmospheric PSFs.

The effectiveness of MFBD depends among other things on the amount of PSF diversity. A lack of diversity can prevent one from obtaining a reliable estimate of the target scene. One scenario in which this might occur is when imaging faint targets such as geosynchronous targets, which can require integration times that greatly exceed the coherence time of the atmosphere. In such cases, the effective PSF is an integrated sum of instantaneous PSF's, which can have a lack of diversity particularly at low spatial frequencies. This can limit the ability of MFBD methods in reliably estimating these frequencies in both the target and individual PSF's. We propose a new

[1] Curvature AO systems have the ability to lock onto targets as faint as MAG +17

approach to overcome this lack of diversity in the case of long exposure imaging, by introducing a variation of the traditional phase diversity imaging methods [1], where instead of injecting a static phase in the diversity channel, we inject a temporally varying phase signal. This injected signal increases the amount of diversity particularly at the low spatial frequencies (Fig. 2). We use knowledge of the injected phase as an additional constraint on the wave-front phase in our MFBD algorithm.

Another limitation of using MFBD methods is the problem of local minima in the solution space. Entrapment in these minima can prevent one from obtaining the true solution to the blind problem. This can often occur when restoring imagery obtained at shorter wavelengths (≤ 0.88 microns), where resolution is high but the turbulence is severe. One approach to overcome this problem is the introduction of wavelength diversity into the data. One accomplishes this by simultaneously observing the target at multiple wavelengths, particularly in the infrared, where though the resolution is poor, the degrading effects of turbulence on the quality of data are less severe. With this multi-wavelength approach, we are able to model the wave-front phase in terms of optical-path-differences (OPD) [2]. These OPD's are common to each wavelength, and when scaled by the wavelength yield wave-front phases at each of the observed wavelengths. This use of common OPD's reduces the problem of local minima, by both incorporating physical constraints on the wave front as well as dramatically reducing the number of estimated PSF parameters.

By overcoming the problem of local minima, we are able to concentrate on the problem of imaging geosynchronous satellites at shorter visible wavelengths. Our motivation is a strong peak in the reflectivity (roughly seven times that in infrared part of the spectrum) of solar panel material at these wavelengths.

We propose a new synergy between instrumentation and blind image restoration that incorporates both wave/phase diversities. Such a synergy will enable reliable estimation of low spatial frequencies and target scene estimation at multiple wavelengths. The former will enable reliable estimation of the low spatial frequencies of both the target scene and PSF, which will yield target scenes with a clean background and low level of artifacts. The latter will facilitate high-resolution imagery of the primary target and confirmation of microsatellites at multiple wavelengths. We show that by using such a synergy one can obtain visible imagery of geo-targets with the AF AEOS 3.6m that has comparable resolution to that of infrared imagery obtained with the University of Arizona 6.5m MMT telescope [3,4]. Furthermore, we show that by recording images of the target simultaneously at multiple wavelengths, one can confirm detection of micro-satellites down to a linear size of 25 cm.

2. MODELING AN ADAPTIVE OPTICS POINT-SPREAD-FUNCTION

To maximize the signal-to-noise ratio (SNR) of observations of faint targets it is common to extend the exposure time of the images beyond the coherence time of the atmosphere. In such case the "long exposure" atmospheric PSF will consist of a central core sitting on top of an extended halo (see Fig 1). To achieve the best sensitivity for target detection in this case, it is important that *both* the core *and* the halo of the resulting AO PSF are correctly modeled. This requires a model with the fewest number of free parameters as possible, and the ability to incorporate prior information on the wave-front phases that may be available from wave-front sensing and wave-diversity/phase diversity data.

We model the point-spread function using,

$$h(x) = \frac{1}{K}\sum_{k}^{K} a_k^*(x) a_k(x)$$

where $a_k(x)$ is the coherent point-spread-function, k is an index that represents a realization of the atmospheric turbulence, and the summation is taken over K (=1 if $T_{int} \leq \tau_0$, else = int(T_{int}/τ_0) realizations. Here T_{int} is the integration time required to observe the target and τ_0 is the coherence (or realization) time for the atmosphere. The coherent PSF is modeled as,

$$a_k(x) = \frac{1}{N^2}\sum_{\rho} A_k(\rho) e^{-i\phi_k(\rho)} e^{-2\pi i \rho \cdot x}$$

Where $A_k(\rho)$ and $\phi_k(\rho)$ are the uncompensated components of the wave-front amplitudes and phases, k is an index that represents a realization of the atmospheric turbulence and N denotes the linear size of the square pixel grid.

3. IMAGING AT MULTIPLE WAVELENGTHS

Imaging a target scene simultaneously at multiple wavelengths enables one to obtain information about materials on the target and to acquire additional constraints on turbulence induced wave perturbations in the telescope pupil. The strength of these perturbations is related to the Fried parameter r_0 parameter, which scales as [5]

$$r_0^V = r_0^I \left(\frac{\lambda_V}{\lambda_I} \right)^{5/6}$$

where λ_V and λ_I denote the observation wavelengths in the visible and infrared respectively, while r_0^V and r_0^I are Fried parameter values at these wavelengths. For multi-wavelength observations the wave-front phase at the j^{th} wavelength can be expressed as,

$$\phi_j(u) = \frac{2\pi}{\lambda_j} W(u)$$

where W(u) denotes the OPD. The phase when expressed in terms of the common OPD, which can be represented using a convenient basis such as Zernike polynomials, can easily be scaled to another wavelength. In MFBD, one can use this fact to estimate the phases at the longer wavelength, where the turbulence is less severe and then scaling these phases to use for estimating the PSF at the shorter wavelength where the turbulence is more severe.

4. TEMPORAL PHASE DIVERSITY

Although AO compensation significantly improves the image SNR, which is of paramount importance when observing faint targets, it also brings a new challenge from the restoration point of view: it produces PSF's that are remarkably similar (see Fig 1).

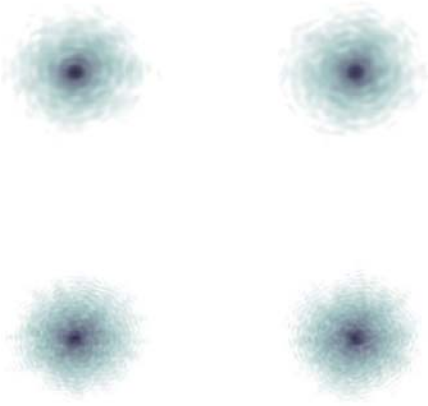

Figure 1 Two realizations of an AO-PSF at infrared (1.6 μm, top) and 'visible' (0.88 μm, bottom) wavelengths. The images are displayed on a logarithmic scale to emphasize the low-level structure. The details of the turbulence conditions are given in Table 1.

Unfortunately, this attribute effectively removes the diversity constraint that is important for the successful restoration of imagery from multi-frame data sets; diversity facilitates estimation of the target that is common to each data frame. Fig 1 highlights an example of this lack of 'PSF diversity'. Here, the similarity of the halo component of the PSF indicates very little diversity in AO-compensated data at the lowest spatial frequencies. This fact makes it difficult to separate the two signals that comprise the measured image (the target and PSF). Practically, this means the fidelity of the restored object and PSFs depends strongly on the initial estimates provided to the restoration algorithm; an extremely undesirable property. To increase the diversity in the PSFs, without an undue decrease in the Strehl ratio[2], as well as strengthen the constraints on the morphology of the PSFs, we propose a new strategy for observing faint objects: 'temporal' phase diversity (a variation of traditional phase diversity in which the aberration injected into the system varies in amplitude with time). From an experimental standpoint, one splits the input light at a given wavelength into two beams, one of which passes through a spatial light modulator that would inject a temporally varying (known) phase aberration into the signal. The effect of this injected signal on the PSF diversity is shown in Fig. 2 where the radially averaged modulus-squared of the OTF is plotted with and without the injected signal.

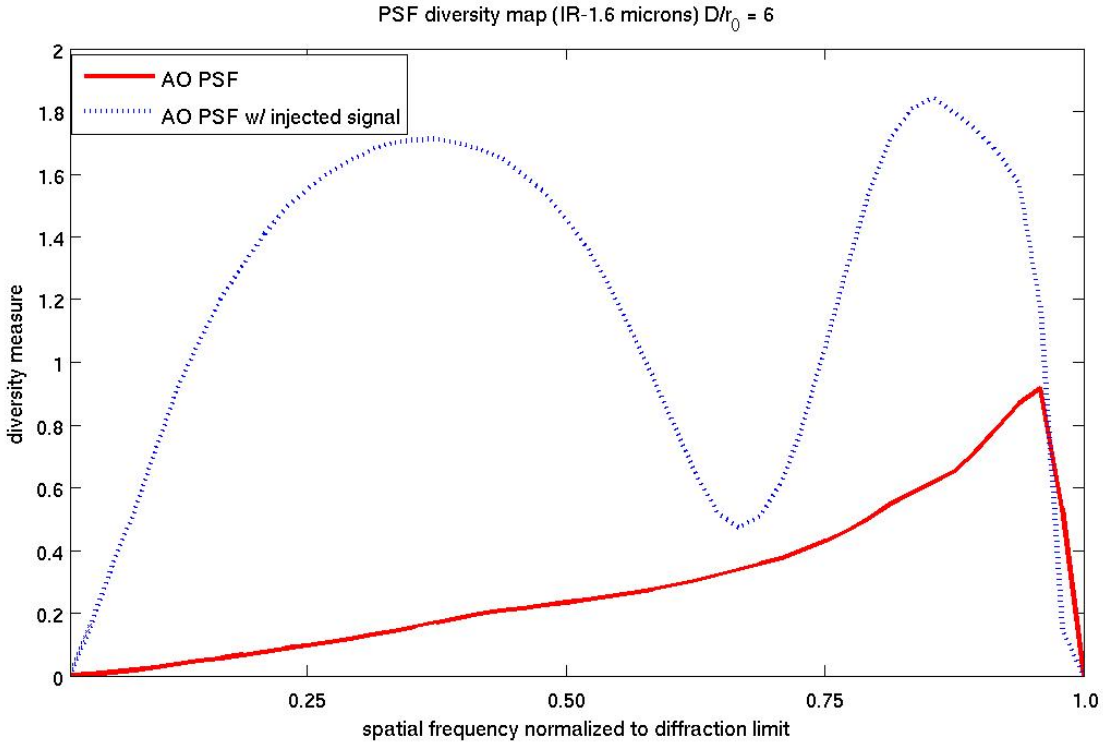

Figure 2 The average energy spectrum of an IR AO-PSF vs. spatial frequency. The solid line denotes the fluctuations (diversity) of the spectra of the AO-PSFs computed from an ensemble of 16 PSFs, and the blue dotted line denotes the diversity after injection of a time-varying phase signal (spherical aberration)

5. RESULTS

Using simulated observations of a GEO target with the AF AEOS 3.6m telescope we demonstrate imaging and detection capabilities when the instrumentation and image restoration have a synergy. Capabilities for a three-second integration on the target is shown in Fig 3. The top left shows the AO "long exposure" image, while the top

[2] The Strehl ratio measures the ratio of the on axis intensity of an observed point source to the theoretical expected intensity for diffraction limited imaging system.

right shows the restored imagery (using current blind restoration methods) using recorded wave-front-sensor (WFS) data as additional prior information. It is clear from this result that WFS data alone is not sufficient to restore AO imagery of a faint geo-target. The use of wave and phase diversity imaging provides additional constraints for solving the blind restoration problem.
Shown in the bottom left is the restoration when combing WFS data with simultaneous observations of the target at 0.880 and 0.440 microns. The restoration using WFS data with both wave and phase diversity is shown in the bottom right. The additional lever provided by the injected diversity facilitates better estimation of the low spatial frequencies of the target, which is evident from the cleaner background and a lesser degree of restoration artifacts.

Including a phase diversity channel reduces the SNR of the data due to the splitting of the incoming photons between the data and diversity channel. We overcome this loss of SNR by extending the total integration of the observations to over a minute. The effects on the quality of the image restoration due to a longer integration time are shown in Fig 4. Here we obtain a high-resolution image of the primary target and detect several micro-satellites in the proximity. Observations at multiple wavelengths provide confirmation on detection of these micro-satellites.

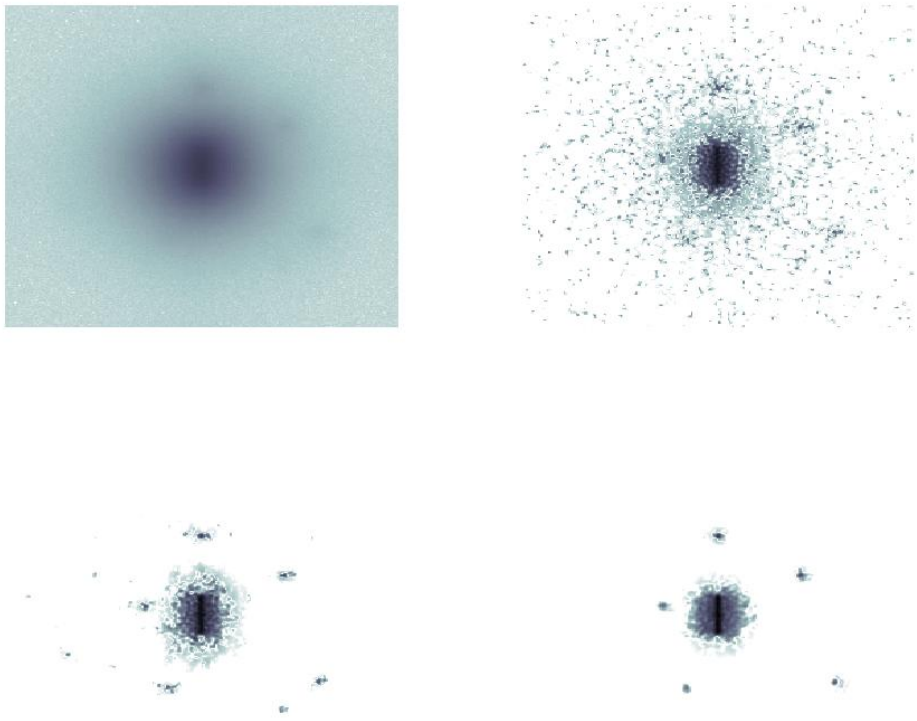

Figure 3 This figure shows the improvements in detection capability when injecting prior information on the wave-front phase into the image restoration process of simulated imagery. Observation wavelength for this imagery is at 0.44 μm. Top left: mean image "long exposure" over 3 seconds. Top right: restored image using recorded wave-front sensing (WFS) data. Bottom Left: restored image using WFS data and wavelength diversity (WD) data. Bottom right: restored image using WFS, WD and phase diverse (PD) data. The raw AO image tentatively shows the presence of two (perhaps three) companions to the main satellite. The restored imagery unambiguously shows the presence of five companions. For the WFS+WD scenario we are able to see the faint 25 cm targets (see appendix for aberration-free image for comparison) but we also see several artifacts. For the WFS+WD+PD scenario, we have lost the ability to see the 25 cm objects (most likely due to the reduction in the SNR of each individual data frame due to the splitting of the photons for phase diversity) but we find a dramatic reduction in the number of artifacts and the level of the residual halo around the main satellite. That is, using all the available constraints improves the resolution and decreases the probability of false detection. Note, the images are displayed on a logarithmic scale to emphasize the low-level structure.

Figure 4. A demonstration of how the detection sensitivity is improved by extending the observation period. Here the restored images, at 0.88 μm (left) and 0.44 μm (right), are based on 77 seconds of simulated data including WFS and wavelength diversity measurements (~ 1,200 256 x 256 pixel images). The 25 cm x 25 cm targets at a distance of 150 m from the main satellite are now identified with a high degree of confidence (i.e., the probability of false detection is low because the target is clearly detected at two widely separated wavelengths). The images are displayed on a logarithmic scale to emphasize the low-level structure.

6. CONCLUSION

We demonstrate how a strong synergy between the instrumentation and image restoration process could enable the use of the AF 3.6m AEOS telescope for observing and monitoring of space-based assets in the geo-synchronous belt. Significant gains in detection sensitivity can be achieved by the injection of prior information on the wave-front phases, via wave-front sensing data and wave/phase-diverse data, into the image restoration process. Acquiring WFS measurements and wave-/phase-diverse data when using the 3.6 m AEOS system would allow us, after image restoration, to obtain resolved imagery of large GEO targets (e.g. communications satellites) and to detect the presence of microsatellites of 50 cm linear size at a distance of 100 m from the main target using 3-seconds worth of data. By extending the integration time to over a minute, targets of 25 cm linear size at a distance of 150 m are clearly detected. Currently, these types of measurement are limited to large aperture telescopes such as the University of Arizona's MMT (6.5 m). However, by a creating a strong synergy between the instrumentation and image restoration we have shown that the AEOS 3.6 m telescope can achieve comparable results at visible wavelengths.

7. APPENDIX: SIMULATION PARAMETERS

We model a geosynchronous satellite based on real observations of the Anik-F2communications and information on the physical size of the Boeing model 702 satellite. The target is the communications satellite ANIK F-2 surrounded by various sized micro-satellites (comprised entirely of solar panels), as observed with a 3.65m telescope equipped with AO such as that at AMOS or STARFIRE.

Turbulence conditions	Kolmogorov turbulence r_0=15 cm, τ_0=12 msec (at 0.5 μm)
Level of AO correction	30% of first 50 modes (Gives a Strehl of 0.10 at 0.880μm and 0.02 at 0.44μm)
Telescope aperture	3.65 m
Observing wavelengths	0.88μm and 0.44μm
Diversity phase	±1 wave of spherical aberration injected as a sinusoidal wave of period 4 secs.
Integration time/frame	384 msec
Total observing time	3secs
CCD read noise	$8e^-$
Main target (Linear size, magnitude)	50m x 5m; mag+9
Micro-satellites (Linear size, magnitude, distance from main target)	See Figure 5

Table 1. Specifications for the parameters used to generate the simulated data.

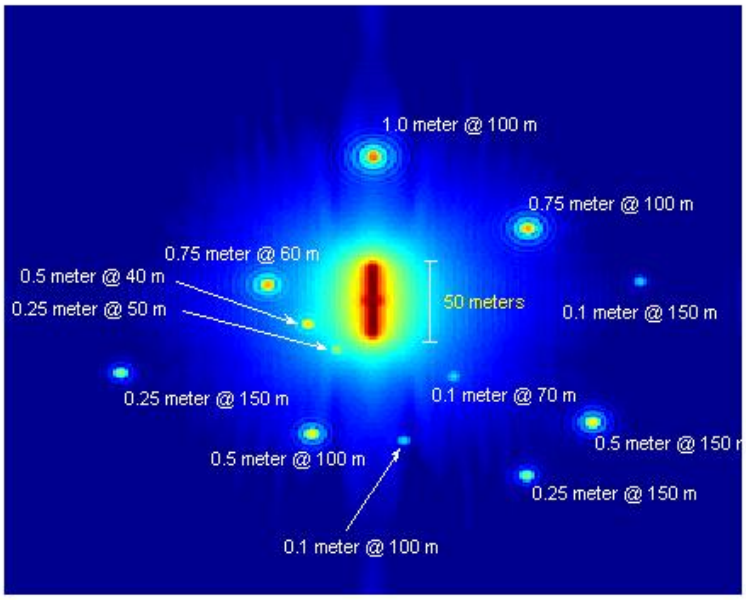

Figure 5 Truth target scene. A model of the Anik-F2 communication satellite is shown surrounded by microsatellites of varying size and distance from primary target

8. REFERENCES

1. R. A. Gonsalves, “Phase retrieval and diversity in adaptive optics”, Opt. Eng. **21**, 829-832 (1982)

2. H. R. Ingleby and D. R. McGaughey, "Real data results with wavelength-diverse blind deconvolution," Opt. Lett. **30**, 489-491 (2005)

3. Worden, S. P., Angel, R. A., Lloyd-Hart, M., Hinz, P., Hege, E. K., Jefferies, S. M. and Hope, D. 2005, “Observing deep space micro-satellites with the MMT and Large Binocular Telescopes”, in *AMOS 2005*, AMOS Technical Conference, Kihei HI, September 2005

4. Roberts, L. C. and Neyman, C. R., “Characterization of the AEOS adaptive optics system”, PASP **114**, 1260-1266 (2002)

5. Roddier, F., “Imaging through the atmosphere,” Adaptive Optics in Astronomy, F.Roddier; editor, 9-24, Cambridge University Press London 1999.